Effect of ventilation design on removal of particles in woodturning workstations

K. Inthavong*, Z.F. Tian, J.Y. Tu

School of Aerospace, Mechanical and Manufacturing Engineering, RMIT University, PO Box 71, Plenty Road, Bundoora, Victoria 3083, Australia

Abstract

Wood processing tasks such as circular sawing and turning that is associated with woodturning operators produce particularly high exposure levels. A computational model including a humanoid and lathe within a test chamber was simulated with monodisperse particles under five different ventilation designs with the aim of reducing the particle suspension within the breathing zone. A commercial CFD code was used to solve the governing equations of motion with a k–ε RNG turbulence model. A discrete Lagrangian model was used to track the particles individually. Measurements to evaluate the efficiency of each ventilation design included total particle clearance and the percentage of particles crossing through the breathing plane. It was concluded that the percentage of particles that cross the breathing plane is of greater significance than the other measurements as it provides a better determination of exposure levels. Ventilation that emanated from the roof and had an angled outlet provided greatest total particle clearance and a low number of particles in the breathing plane. It was also found that the obstruction from the local roof ventilations caused separation of the air that flowed along the ceiling to produce a complex flow region. This study provides a basis for further investigation into the effects of particle size and density on the particle flow patterns and potential inhalation conditions for a given ventilation design.
© 2008 Elsevier Ltd. All rights reserved.

Keywords: Wood dust; Particle clearance; Simulation; CFD; Building; Woodturning

1. Introduction

Wood dust is one of the most common organic dusts in which humans are exposed to due to the extensive use of wood for construction material and furniture [1]. The International Agency for Research on Cancer estimated that at least two million people in the world are exposed to wood dust occupationally [2]. Studies have found that exposure to wood dust can cause health effects from nasal mucosa damage, irritation and sino-nasal cancer to deep lung deposition leading to lung cancer and impaired respiratory function. Wood processing tasks such as circular sawing, turning and sanding that are common among woodturning operators, cabinet makers and carpenters produce particularly high exposure levels [3,4]. Determinants of wood dust exposure include the airflow

field in the working area, subject inhalation rate and ventilation systems while the level and pattern of toxicity varies with the characteristics of the wood dust such as the type of wood, size, shape and density.

Chung et al. [5] measured the characteristics of wood dust particles in terms of their density and size distribution for a variety of wood types and under different wood processing methods, such as sawing and sanding. The size of dust particles is significant when assessing their likely deposition in the airways. According to Wickham [6] particles greater than 3 μm deposit mainly in the upper respiratory system while particles that reach the lower parts of the lungs are predominantly between 1 and 3 μm. Submicron particles around less than 0.4 μm will deposit by diffusion. The inhalation of wood dust through the nasal cavity has been simulated by Tian et al. [7] which injected the wood dust particles from the size distribution given by Chung [5]. It was found that the particles deposited in the anterior regions of the nasal cavity, caused by inertial impaction. The simulation used a particle size distribution that had settled on the

---

*Corresponding author. Tel.: +61 3 9925 6191; fax: +61 3 9925 6108.
 E-mail addresses: Jiyuan.Tu@rmit.edu.au,
s3113652@student.rmit.edu.au (K. Inthavong).

Nomenclature

ACH	air change per hour
C_D	drag coefficient
d_{ae}	aerodynamic diameter
d_g	geometric diameter
F_D	drag force
F_s	additional forces (source term)
k	turbulence kinetic energy
P	pressure
Re	Reynolds number
S	strain rate tensor
u	velocity
U	average velocity

Greek symbols

ρ	density
δ	Kronecker delta function
ε	turbulence dissipation
μ	dynamic viscosity
μ_t	turbulent eddy viscosity

Subscripts

i,j	tensor subscripts
g	gas phase
p	particle phase

ground rather than the particle size distribution suspended in the breathing region of the worker. A fully integrated approach is therefore needed to evaluate the deposition of particles in the nasal cavity that includes the generation of wood dust from the wood processing stage, wood type and the effects of ventilation design which will provide a better particle size distribution found in the breathing region of the worker. In this initial study, however, only the airflow patterns and the wood dust removal from a wood turning station are studied from different ventilation designs.

Legislation among developed nations put in place preventative measures such as the occupational exposure limits and the employment of ventilation systems which provide significant influence on the occupational health. The use of local exhaust ventilation is a common method to control contaminants in buildings with localised emissions. Indoor airflow and particle dispersion have been studied by many authors [8–11]. From these studies it was found that (i) the particle distribution pattern from a downstream point source is strongly dependent on the ventilation air supply rate and (ii) particle deposition and migration are mainly influenced by the particle properties, the ventilation conditions and airflow patterns. This paper presents the modelling capability of computational fluid dynamics (CFD) to determine the best ventilation design from a group of selected designs. An actual woodturning work-station at the, '*Peninsula Woodturners Guild Incorporated*' in Victoria, Australia was used to develop a realistic computational lathe and humanoid surface mesh model. Woodturners face a problem in which the wood dust generated by the lathe machine drifts around the room and is not adequately cleared by the current air ventilation system. Therefore, analyses on the airflow pattern and particle distribution especially around the breathing area of a woodturner were carried out using the commercial software FLUENT 6.3 (Ansys Inc.). The concentration levels of the wood dust particles that flowed within the breathing region of the woodturner can then be used to evaluate the likelihood of inhalation and finally predicted deposition sites within the respiratory system.

2. Numerical procedure

2.1. Geometrical models

In the modelling phase, a control test chamber was developed and used to validate the computational model based on an actual workshop. A humanoid, lathe and different ventilation configurations were then created and placed into the control test chamber. The models were created using the surface and wireframe design function within CATIA V5 (Dassault Systémes) before being exported as IGES files for meshing within GAMBIT (Ansys Inc.). The configuration and dimensions of the test chamber (5.17 m × 3.64 m × 2.19 m) are shown in Fig. 1 which is similar to the experimental model investigated by Madsen et al. [12]. Three models with mesh densities of 85k, 175k and 293k cells were incrementally developed through refinements at the near walls, inlet and outlet regions. Four lines along the symmetry plane through the middle of the test chamber (Fig. 1) were created and used for validation and grid independence. The humanoid and lathe model that was initially developed in CATIA V5 was slightly adapted due to data loss during the conversion stage from a solid model (IGES) into a meshed model within GAMBIT as shown in Fig. 2.

2.2. Ventilation designs

Five different ventilation designs were considered. The conditions and classifications for the designs are summarised in Table 1 and shown in Fig. 3. The local ventilation design acting as an exhaust outlet has dimensions of 0.2 m × 0.2 m. The global exhaust outlet positioned on the roof is defined as a pressure outlet with dimensions of 0.1 m × 0.1 m, while the inlet vent is defined as a velocity inlet with dimensions of 0.2 m × 0.46 m and is located on the wall behind the humanoid for all the designs. Note that only one of the local ventilation configurations is present at one time during a simulation despite all five configurations being superimposed into Fig. 3. The ventilation configura-

tions differ through the positioning and direction of the local outlet vent in relation to the lathe with the aim of reducing the particle suspension within the breathing zone. The position of the local outlets can be categorised into two groups; a local outlet emanating from the roof positioned directly above the lathe machine (R1, R2, R3) and a local outlet emanating from the floor (F1, F2). The configuration F2 is the most commonly used design and is the one that is currently in place at the *Peninsula Woodturners Guild* workshop that is under investigation.

2.3. Fluid phase modelling

The inlet provides the flux of air from the outer environment passing through the room. During a site visit to the *Peninsula Woodturners Guild* it was found that the inlet flow rate was quite low which may be a cause of complaints of poor ventilation. For simulation, the air flowed into the test room was assumed to have a velocity inlet of $0.64\,\text{m/s}$ ($Re \approx 18,000$, ACH $= 5.2\,\text{h}^{-1}$) and flows out at the global outlet at ACH $= 1.16\,\text{h}^{-1}$ and at the local
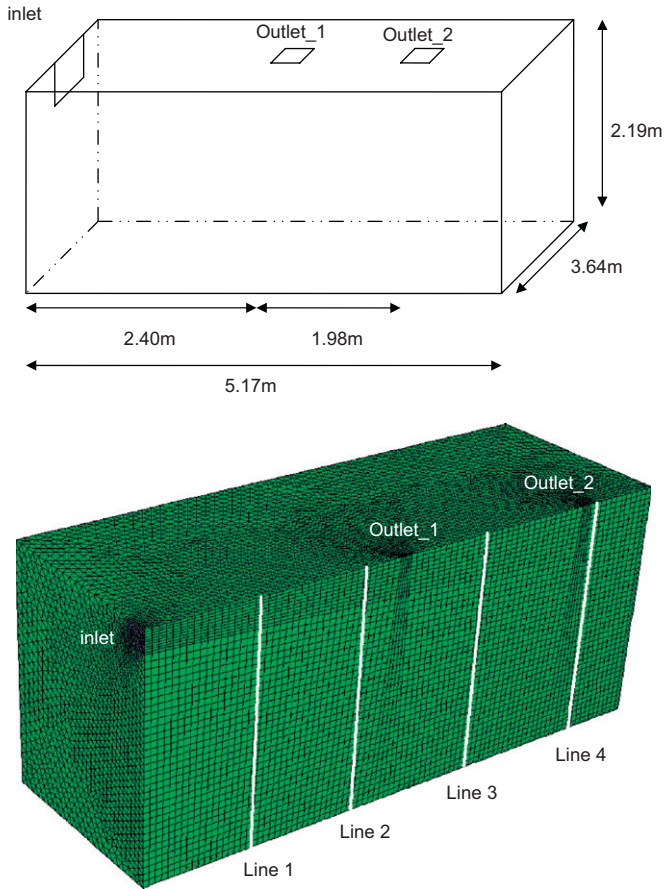

Fig. 1. Test chamber geometry and mesh. Four lines along the symmetry are created to obtain velocity profiles for validation of the model.

Table 1
Description of different ventilation designs

| Ventilation	Location from	Description
R1	Roof	Directly above the lathe machine, in close proximity with the humanoid
R2	Roof	Vertically aligned with the lathe but offset by a further 500 mm from R1 in the direction away from the humanoid
R3	Roof	Offset by 500 mm from R1 in the direction away from the humanoid with a 45° angle such that the exhaust vent is directed at the workpiece attached to the lathe machine
F2	Floor	Level with the table of which the lathe machine is mounted. This is the actual configuration currently in use at the workshop
F3	Floor	A cowling is installed so that the outlet vent is facing the humanoid directly
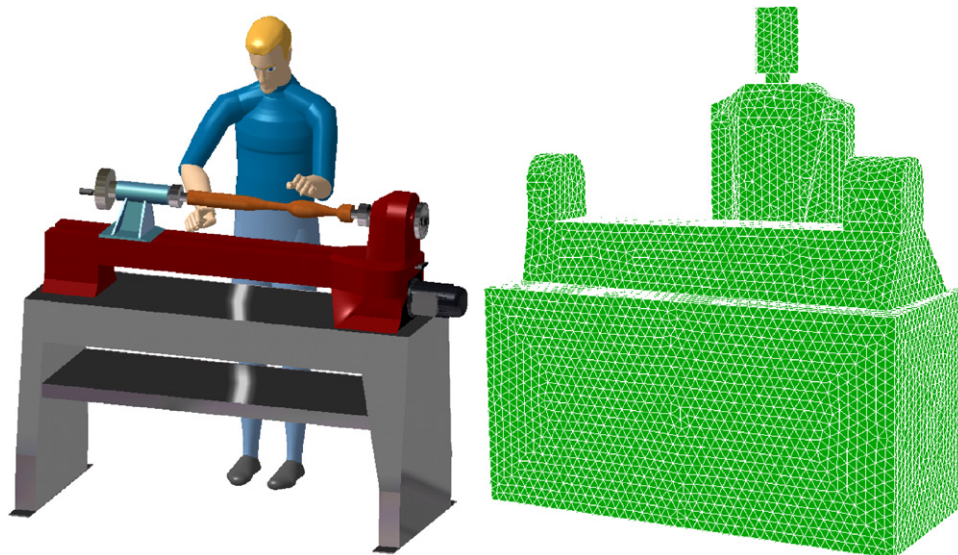
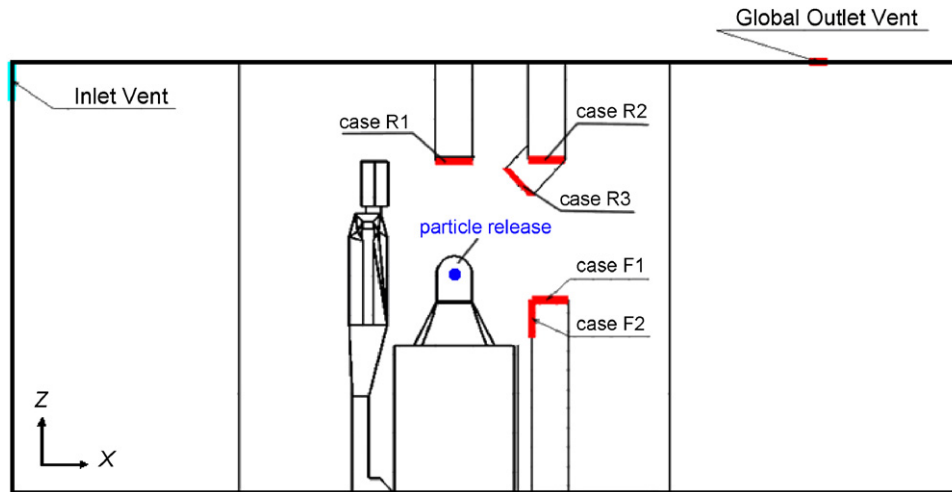Fig. 2. Solid and meshed computational models of the humanoid and lathe.

Fig. 3. Five local ventilation outlets used for analysis. Three outlets emanate from the roof while two from the floor.

outlet at $\text{ACH} = 4.04\,\text{h}^{-1}$. The flow was assumed to be isothermal and steady. This assumption was made in order to focus on the effect of ventilation designs independent of the variables such as convection caused by heat transfer from the human body during winter (more clothing) and summer (less clothing) and flows caused by movement of the human. Therefore, the results presented are purely at an isothermal state and the effects of convective heat transfer can be found in separate works by Deevey et al. [13], Murakami et al. [14] and Murakami [15]. Under these conditions and similar to [11–13] an assumed turbulent flow regime was used. The Reynolds-Averaged Navier–Stokes based k–ε turbulent model equations for a turbulent fluid flow was used and can be written as follows:

$$\frac{\partial U_i}{\partial x_i} = 0, \tag{1}$$

$$\frac{\partial U_j U_i}{\partial x_j} = -\frac{\partial P}{\partial x_i} + \mu\nabla^2 U_i + \frac{\partial}{\partial x_j}\left(-\rho\overline{u_j' u_i'}\right), \tag{2}$$

$-\rho\overline{u_j' u_i'}$ is a second moment statistical correlation called the Reynolds stresses which need to be modelled to close the system of equations as it is an unknown. The Reynolds stresses can be approximated by using the Boussinesq assumption where

$$-\rho\overline{u_j' u_i'} = -2\mu_t S_{ij} + \tfrac{2}{3}\delta_{ij}\rho k. \tag{3}$$

Two additional transport equations for k and ε are needed.

$$\frac{\partial(\rho U_j k)}{\partial x_j} = \left(\mu + \frac{\mu_t}{\sigma_k}\right)\nabla^2 k + \mu_t S^2 - \rho\varepsilon, \tag{4}$$

$$\frac{\partial(\rho U_j \varepsilon)}{\partial x_j} = \left(\mu + \frac{\mu_t}{\sigma_\varepsilon}\right)\nabla^2\varepsilon + C_{\varepsilon 1}\frac{\varepsilon}{k}\mu_t S^2 - C_{\varepsilon 2}^*\rho\frac{\varepsilon^2}{k}, \tag{5}$$

where $\eta = (2S_{ij}S_{ij})^{0.5}k/\varepsilon$, $C_{\varepsilon 1} = 1.42$ and $C_{\varepsilon 2}^* = 1.68 + 0.0845\eta^3(1 - \eta/\eta_0)/(1 + 0.012\eta^3)$.

These equations were discretised using FLUENT 6.3, a finite volume solver used under the segregated scheme. The

third-order accurate QUICK scheme was used to approximate the momentum equation whilst the pressure–velocity coupling was solved through the SIMPLE method. The convergence criteria for the air phase properties (resolved velocities and pressure) were 10^{-5}. The adequacy of the convergence criteria was further checked by comparing the simulation of airflows along the lines at the symmetry (Fig. 1) with the convergence criteria values of 10^{-5} and 10^{-7}. The difference between the air velocity profiles between the two simulations was negligible.

2.4. Particle phase modelling

For a low volume fraction of dispersed second phase (particle), an Eulerian–Lagrangian approach was used. This allows the effects of turbulence modulation (effect of particles on turbulence) to be neglected. The Lagrangian approach splits the particle phase into a representative set of discrete individual particles and tracks these particles separately through the flow domain by solving the equations of particle movement. Assumptions regarding the particle phase included the following: (i) no particle rebounded off the walls/surfaces as wood dust tend to be soft and flaky; (ii) no particle coagulation in the particle deposition process and (iii) all particles are spherical solid shapes. Trajectories of individual particles can be tracked by integrating the force balance equations on the particle.

$$\frac{du_p}{dt} = F_D(u_g - u_p) + \frac{g(\rho_p - \rho_g)}{\rho_p} + F_s, \tag{6}$$

$F_D(u_g - u_p)$ is the drag force per unit particle mass where:

$$F_D = \frac{18\mu_g}{\rho_p d_p^2}\frac{C_D Re_p}{24}, \tag{7}$$

Re_p is the particle Reynolds number defined as:

$$Re_p = \frac{\rho_p d_p|u_p - u_g|}{\mu_g}. \tag{8}$$

The drag coefficient C_D is given as

$$C_D = a_1 + \frac{a_2}{Re_p} + \frac{a_3}{Re_p^2},\tag{9}$$

where the a's are empirical constants for smooth spherical particles over several ranges of particle Reynolds number [16]. The second term in Eq. (6) is the gravity term while the third term, F_s represents other possible forces such as virtual mass force, Basset force, pressure gradient force, lift force, thermophoretic force and Brownian force. Firstly, the Brownian force can be neglected, since these effects should only be included for sub-micron particles only [17]. Secondly, the particulate material considered is far denser than air, causing terms that depend on the density ratio, such as the pressure force, buoyancy force, virtual mass effect and Basset force to be very small [18]. Finally, the Saffman's lift force is not included due to relatively large particles and low-level fluid shear fields. Moreover, the work by Li and Ahmadi [19] showed that it is only recommended to include this force for sub-micron particles. The CFD code, FLUENT, handles the turbulent dispersion of particles by integrating the trajectory equations for individual particles, using the instantaneous fluid velocity, $u_i^g + u_i'(t)$, along the particle path during the integration process. Here, the discrete random walk (DRW) model is used where the fluctuating velocity components u_i' that prevail during the lifetime of the turbulent eddy are sampled by assuming that they obey a Gaussian probability distribution. Details of the model can be found with the FLUENT user guide.

To ensure confidence in the Lagrangian model, a few steps were undertaken. Firstly, the number of parcels used were evenly spaced apart which were stochastically determined with 120 repetitions. An increase in the turbulent dispersions to 300 repetitions per particle stream found a change in particle deposition of less than 2%. Secondly, each individual particle was tracked and recorded as it passed through defined planes within a breathing region and a middle cross-sectional plane (described in more detail in Section 3.2). For small particles, the DRW model used in this study may have a deficiency when the k–ε models are employed for the gas phase. In strongly inhomogeneous diffusion-dominated flows where small particles should become uniformly distributed, DRW combining with k–ε models may predict high concentration in low-turbulence region of the flow [20]. Nevertheless, no evidence of this unphysical phenomenon have been found in this study. However, in the case that particles are caught in a low-turbulence recirculating region, they may be tracked infinitely as the Lagrangian tracking terminates when a particle escapes through the outlets or touches a surface that is set to trap. This can cause an unrealistic value for number of particles that may pass through a plane. The test for unrealistic particles passing through a plane was made by undertaking a sensitivity test. The trajectory of the turbulent particle dispersion within the DRW model is based on an integral time scale and a maximum number of steps allowed for tracking. Particles that do not terminate within the tracking limit are counted as incomplete and these particles are assumed to be caught recirculating. However, if not enough steps are defined then some particles that are not recirculating may also not complete their trajectory. Therefore, to eliminate this, the smallest value for the maximum of steps was chosen where the number of incomplete particles does not change.

2.5. Boundary conditions

Generally wood dusts can be categorised into softwoods and hardwoods. Hardwoods are primarily angiosperms (having broad leaves and are deciduous) such as oak, while softwoods are gymnosperms (having needle-like leaves) such as pine. The classification terms refer to the species and not necessarily the hardness although hardwoods tend to be denser than softwoods. The processing of the raw timber from the use of high-powered reciprocating tools such as sanding and sawmills generates large quantities of fine inhalable wood dust. Since this paper's focus is on ventilation design, only one particle type will be considered; wood dust particles from pine. The work by Chung et al. [5] determined the particle size distribution of dusts during sawing of pine where the density was $560\,\text{kg/m}^3$. The particles were simulated as a set of 10 discrete particle sizes with each particle size skewed to account for its distribution. The simulated particle size distribution is given in Fig. 4. Under the statistically stable number of turbulent dispersions per particle stream, a total of 80,000 particle streams were used for the polydisperse set of particles to obtain the quantitative results, while a reduced number of particles was used to allow better visualisation for the qualitative results. The particles were released evenly along the lathe (Fig. 3) with velocities of 3 m/s in the X- and Z-directions, which is the direction diagonally upwards and away from the humanoid. The equivalent aerodynamic diameter, d_{ae}, is defined as
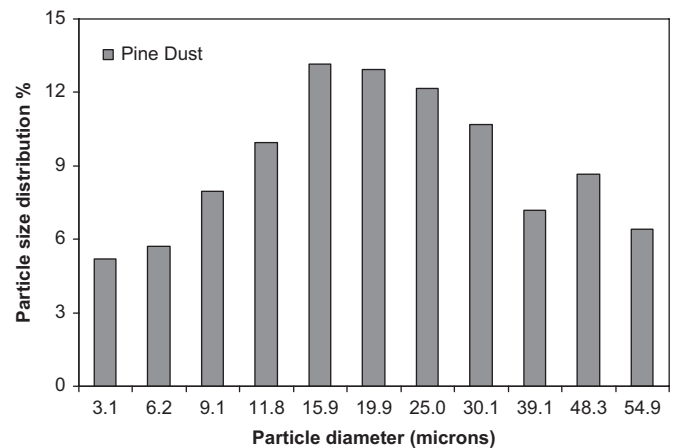
$$d_{ae} = d_g \sqrt{\rho_p/1000}.\tag{10}$$

Fig. 4. Simulated particle size distribution based on the experimental work of Chung et al. [5].

For pine dust with density of 560 kg/m^3 and size range of 3–55 μm, this equates to a range of 2–41 μm. In still air, particles with d_{ae} that are smaller than 1 μm are likely to be found suspended in the air, while particles with d_{ae} from 1 to 10 μm tend to settle by gravity. However, normal air movements that are typically found in indoor workshops have shown that particles are often suspended in the air for a long period of time. This includes particles with d_{ae} larger than 10 μm found in the air near the dust source and under strong wind conditions [21]. Moreover, the inhalability of ultralarge particles in still air conducted by Dai et al. [22] confirmed that the 'cut-off' particle size for nasal inhalation is approximately 135 μm.

3. Results and discussion

3.1. Mesh independence and validation

A mesh independence test was performed to ensure that the solution did not change when further refinements of the mesh were made. Velocity profiles were taken along the lines from Fig. 1 for comparison. The profiles converged between the 175,000 cell model and the 293,000 cell model and subsequently the 293,000 cell model was used for the remaining study. Validation of the computational model implementing the k–ε RNG turbulence model was also checked against other RANS-based turbulence models. While the three different RANS-based turbulence models provided similar velocity profiles, the RNG turbulence model produced the most matching profiles with the experimental measurements by Madsen et al. [12] across the four lines (Fig. 5). The slightly better performance by the RNG model is consistent with other findings in literature [10,23,24] for similar geometries.

3.2. Airflow from different ventilation designs

Two cross-sectional planes were created to obtain velocity vector and contour plots (Fig. 6). The y-midplane cuts through the middle of the Y-axis and captures the outline of the ventilation designs and the air that flows across the plane. The breathing plane was chosen as it is located within the breathing region of the humanoid. The plane is approximately 18 cm in front of the humanoid.
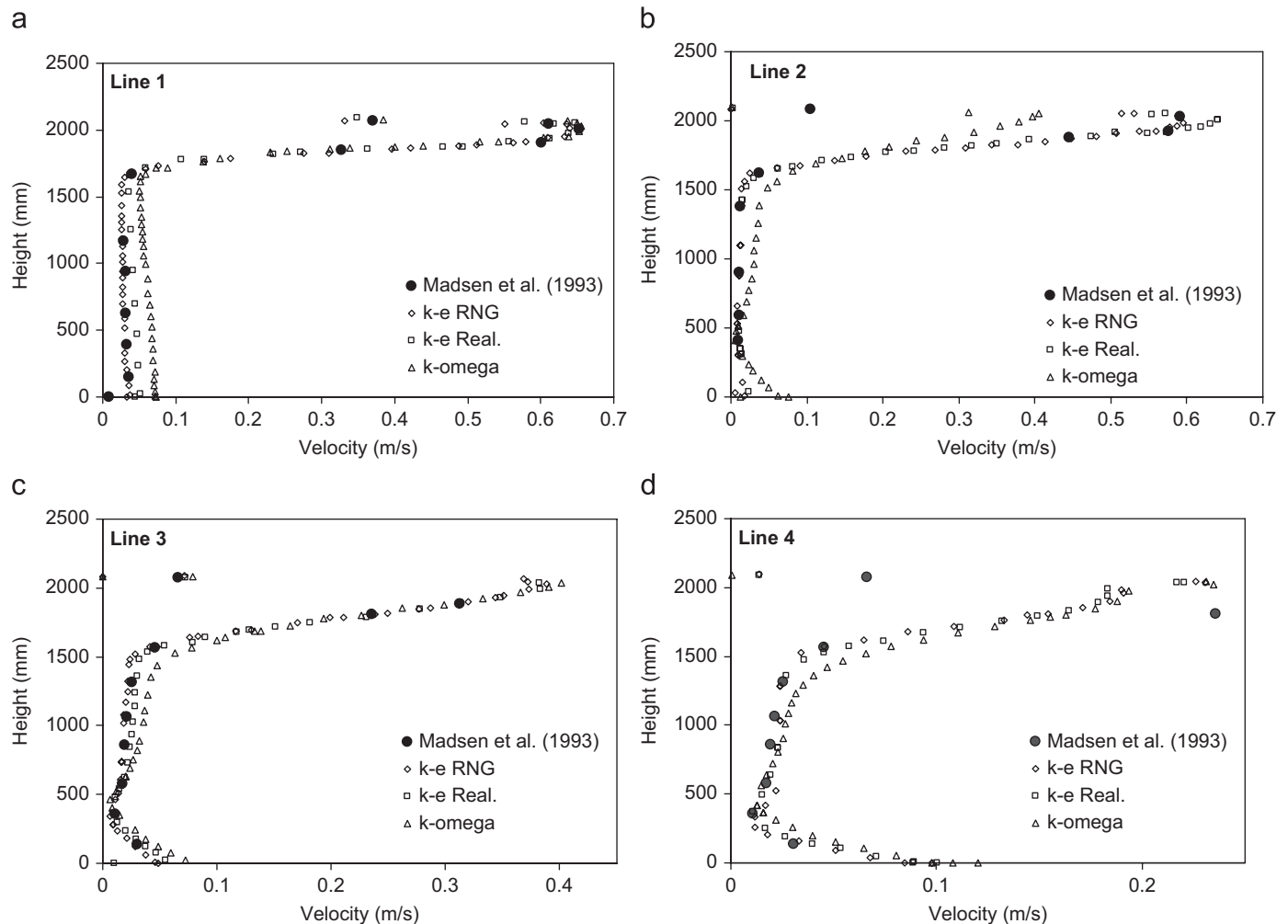

Fig. 5. Velocity profile comparison at four lines for different turbulence models. (a) Velocity profile along symmetry plane at Line 1; (b) velocity profile along symmetry plane at Line 2; (c) velocity profile along symmetry plane at Line 3; (d) velocity profile along symmetry plane at Line 4.
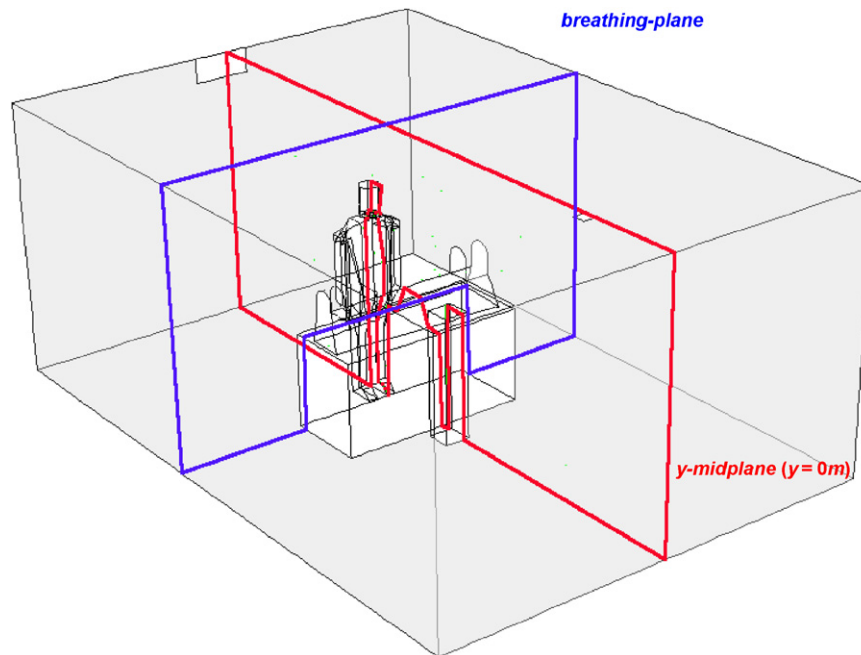
Fig. 6. Two orthogonal planes, breathing plane and *y*-midplane used to determine the percentage of particles passing through the planes.

This plane is used to measure the amount of wood dust that is recirculated towards the breathing region of the humanoid caused by the airflow. A combined contour plot of the axial velocity (*x*-direction) and the streamlines was used to visualise the airflow field for the three cases R1, F1 and F2. The other configurations R2 and R3 show similar flow patterns to R1 and the qualitative images are not shown for brevity. The black contour colour represents maximum reverse flow (−0.3 m/s), the white colour represents stagnant flow (0 m/s) and the red colour represents maximum positive flow (0.6 m/s). The contours in all the airflow visualisation plots share the same contour colour scheme and scale given in Fig. 7a.

The major difference in flow patterns between the local roof ventilation (R1, R2, R3) and the local floor ventilation (F1, F2) is the obstruction to the bulk flow by the vents emanating from the roof. For the configurations where the ventilation is from the roof the bulk flow moves steadily across the ceiling before it encounters the outlet vents. At this region, the flow separates and disperses in all directions around the vent. The size and geometry of the local outlet vent limits the amount of flow that can exit to approximately 75% while the remaining bulk airflow continues, merging back together behind the local vent before exiting at the general outlet vent further downstream. A small region of recirculation is found immediately behind the outlet vent and an even smaller one just behind the lathe. A major region of recirculation is found at the open space downstream of the lathe where low flow regions occur. The air flow where the breathing region and where the particles are released, show streamlines pointing directly upwards caused by the recirculating air that comes from the floors and upwards. This increases the likelihood of particles

drifting into the breathing region. Ventilation R3 which is further away from the humanoid than R1 (Fig. 3) causes the flow to be directed away from the breathing region. This creates a reduction in the likelihood of particles to drift towards the humanoid. For ventilations that emanate from the floor, the flow patterns in the breathing region are significantly influenced by the downstream recirculation.

For the F1 case, the reverse flow travels from a downstream position towards the local outlet and is able to exit as the air flows over the outlet. This air is met by flow in the opposing direction that comes from a vortex found near the head of the humanoid. The outer streamlines of the vortex that flow outwards are mainly directed away from the humanoid. Also, the negative axial velocity found in the breathing region is small. In comparison, the F2 case has the outlet facing the opposite direction to the downstream reverse flow. The air has to travel back past the outlet and then turn 180° to exit at the outlet vent. Not all the air will be able to escape by this method and a majority will actually flow past the outlet before recirculating again. A stagnation point is found above the lathe where the flow is directed outwards in all directions, with which a majority is pointing directly back at the humanoid. This undesirable effect will enhance the inhalability of the wood dust particles generated. The negative axial velocity found in the breathing region is larger in the F2 case in comparison with F1. By taking the same contour and streamline plot at a different plane, *y* = −0.1 m (at the side edge of the local outlet vent), the effects of the local outlet locations are emphasised (Fig. 8). The streamlines clearly show how the reverse flow is much stronger in F2 causing the flow to be directed at the humanoid. In contrast, the vortex near the humanoid found
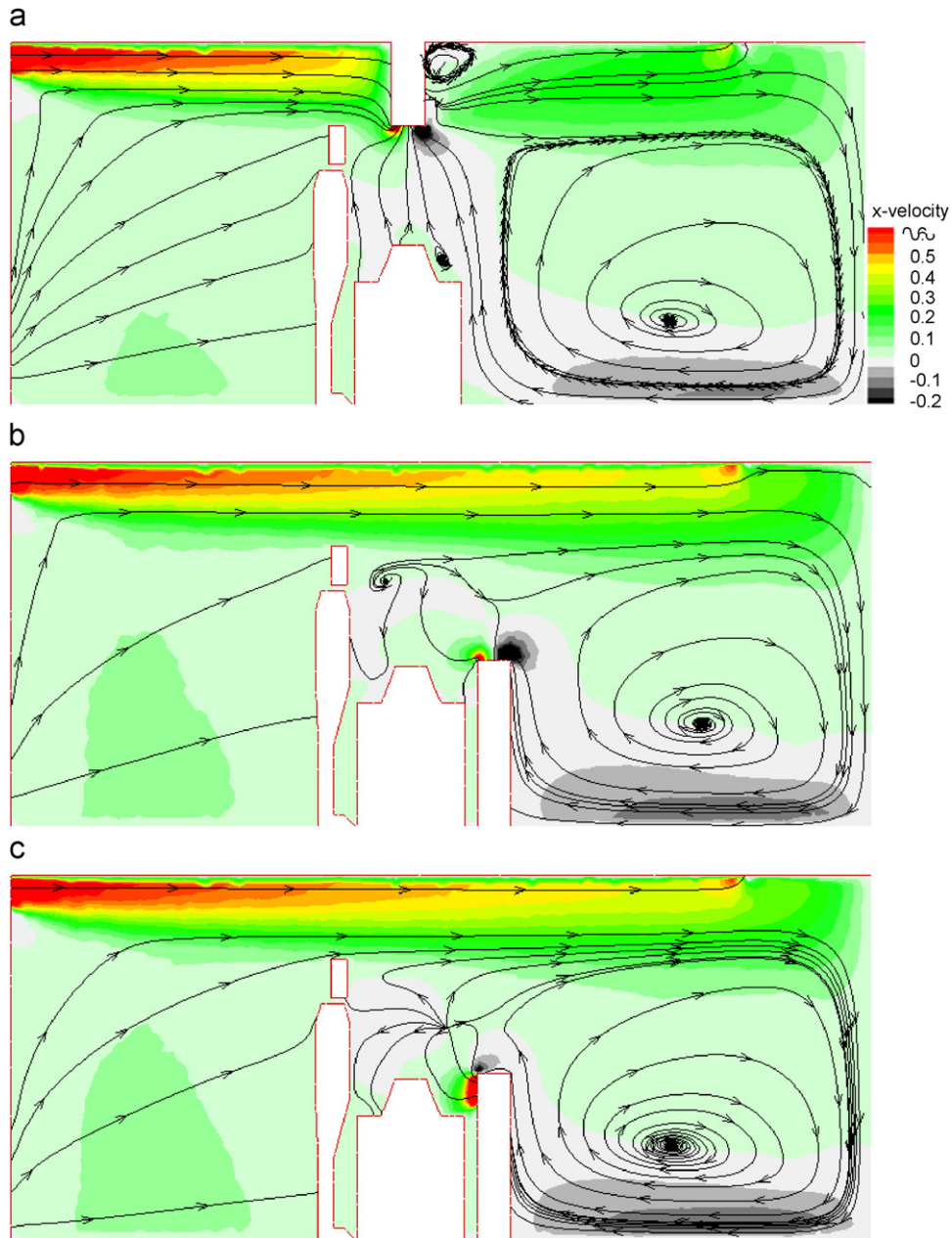
Fig. 7. Streamlines and axial velocity contours at the y-midplane (y = 0 m) for three different ventilation designs (a) R1, (b) F1 and (c) F2.

in F1 show streamlines pointing downwards pushing the particles away from the humanoid. This flow feature will have a considerable influence on the particle trajectories and clearance. It is also noted that F2 is the current design commonly found at the workshops and is indeed the design currently used at the *Peninsula Woodturners Guild*. This flow field may be an explanation as to the complaints issued by the organisation regarding the efficiency of the local ventilation.

3.3. Particle distribution

Wood dust particles were released from the lathe under five ventilation configurations as found in Fig. 3. The

clearance of the particles from the working environment is an important parameter when considering the effectiveness of ventilation designs for safer occupational health. The particles were deemed to have been cleared from the working environment if the particles passed through the local or the general outlet vents. Additionally, the number and location of the particles that passed through the breathing plane or the y-midplane (Fig. 6) were recorded by applying a small subroutine that was implemented into the FLUENT user defined functions. The normalised percentage of particles that pass through the breathing plane is defined as

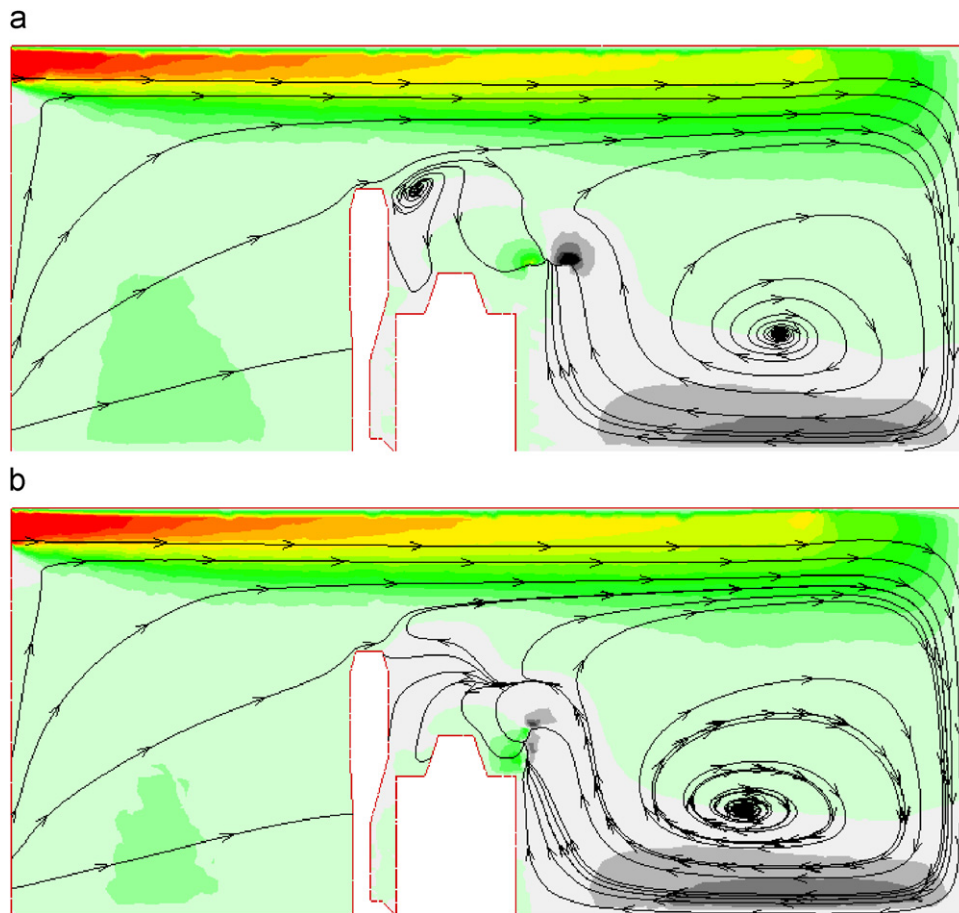$$\%_{\text{normalised}} = \frac{n_{\text{ventilation}}}{n_{\text{max}}}, \tag{11}$$

Fig. 8. Streamlines and axial velocity contours at the y-midplane ($y = -0.1$ m) for three different ventilation designs (a) F1, (b) F2.

where the number of particles passing through a plane was normalised by the maximum number of particles that passed through one plane. In this instance, the maximum occurred for ventilation R2. A high value of the normalised percentage of particles passing through the breathing plane suggests that the effects of recirculation are significant enough to transport the particles in the reverse direction to the bulk flow. Furthermore, a high percentage of particles in the breathing plane is unsatisfactory as exposure to the wood dust is more profound and the likelihood of inhalation by the worker is enhanced. This parameter may be considered even more important than the number of particles that are cleared through the outlet vents. The number of particles passing through the y-midplane shows the dispersion of the particles in relation to the airflow direction. One minor discussion point for these measurements is that the number of particles that pass through a plane does not necessarily reflect the total number of individual particles. For example, a particle that is caught in a recirculating region will pass through a plane in one direction, recirculate and then will pass through the same plane again. Therefore, recirculating regions close to the humanoid or the breathing zone should be avoided as it enhances the number of exposures to the particles.

Fig. 10 summarises the performance of the ventilation designs in terms of the particle clearance and the percentage of particles that pass through the y-midplane and the breathing plane. Ventilation F2, where the outlet vent is close to the lathe, provides the best clearance of particles. However, it also produces the highest percentage of particles passing through the breathing plane. This suggests that there are high recirculating airflows that induce particle movement in the breathing areas. Fig. 9 shows that the close arrangement of the outlet vent induces a large number of particles to exit. However, the size of the outlet vent, (hydraulic diameter $D_h = 0.2$ m) will limit the amount of particles that can exit the vent at a given time. The airflow and particles that cannot exit due to the limiting local outlet vent are then forced backwards recirculating or join the bulk flow that travels along the ceiling. An improvement to the ventilation designs that may be tested in future is to increase the D_h of the local outlet vent. Ventilation F1 showed improvement over F2 in relation to the percentage of particles that flowed through the breathing plane (2% compared to 37%), although the total number of particles cleared for F1 is less than F2 (75% compared to 88%).

Although ventilations F1 and F2 both emanate from the floor, the percentages of particles passing through the
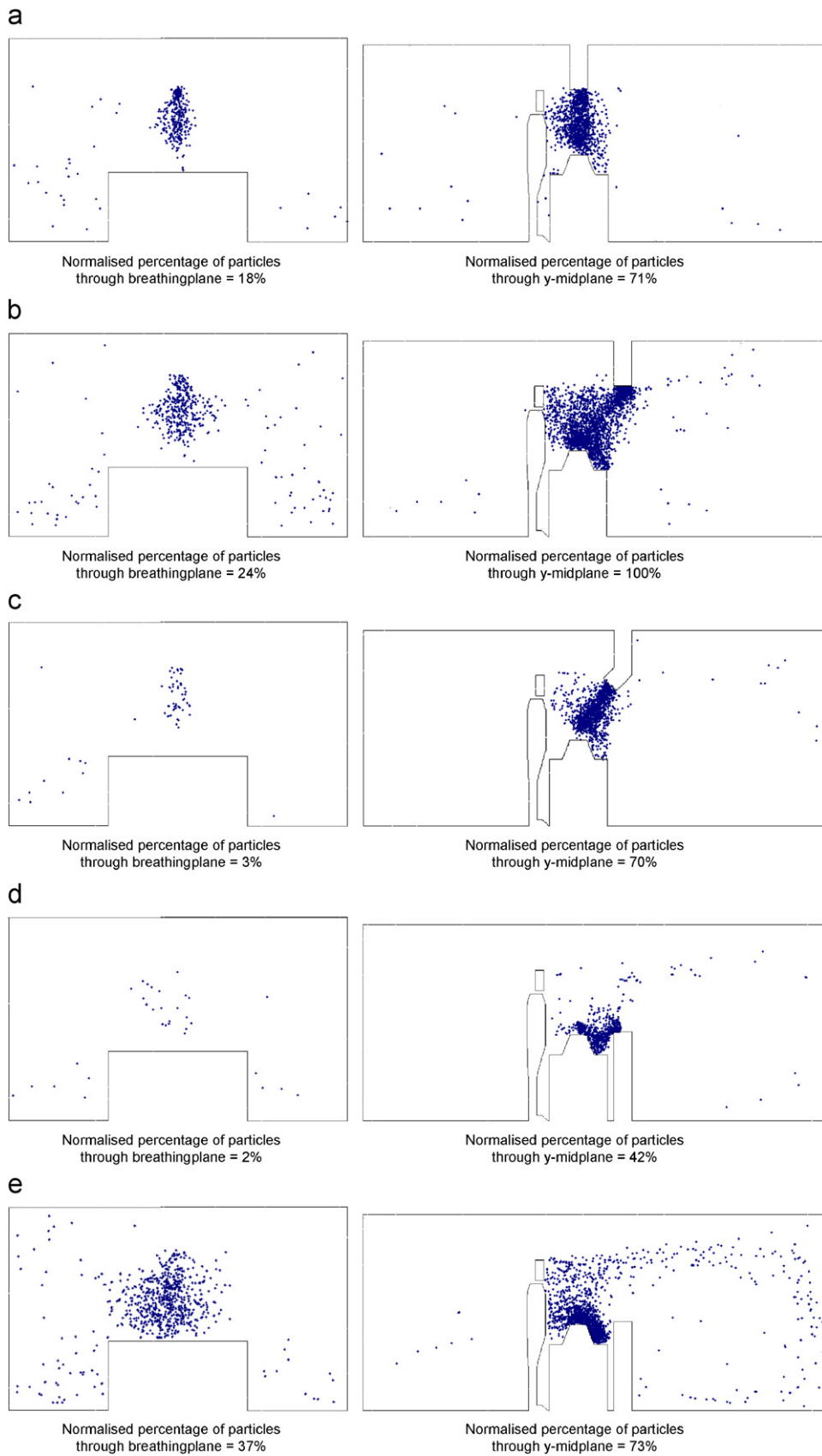
a

Normalised percentage of particles
through breathingplane = 18%

Normalised percentage of particles
through y-midplane = 71%

b

Normalised percentage of particles
through breathingplane = 24%

Normalised percentage of particles
through y-midplane = 100%

c

Normalised percentage of particles
through breathingplane = 3%

Normalised percentage of particles
through y-midplane = 70%

d

Normalised percentage of particles
through breathingplane = 2%

Normalised percentage of particles
through y-midplane = 42%

e

Normalised percentage of particles
through breathingplane = 37%

Normalised percentage of particles
through y-midplane = 73%

Fig. 9. Percentage of particles passing through the breathing plane and the y-midplane for different ventilation conditions. (a) R1 ventilation; (b) R2 ventilation; (c) R3 ventilation; (d) F1 ventilation; (e) F2 ventilation.
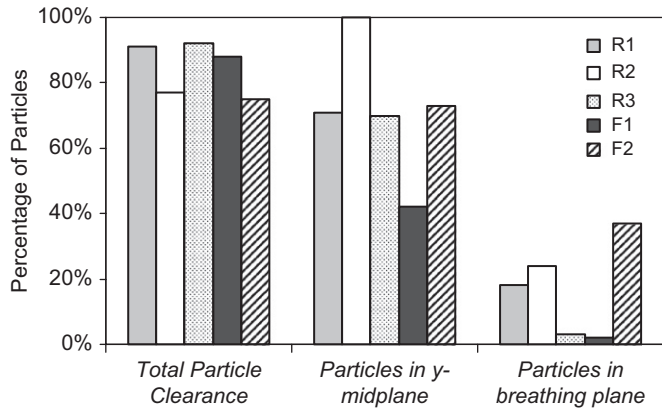
Fig. 10. Ventilation performance in terms of particle clearance and particles passing through the y-midplane and the breathing plane.

planes are markedly different. It was found earlier in Fig. 8 that the streamlines for F1 were favourable for clearance of particles away from the humanoid while F2 showed streamlines directed at the humanoid. F1 showed the smallest percentage of particles crossing through the two planes which means that the particles are less likely to be found suspended in the air and will either be trapped on surfaces or exit through the outlet vents in a short period of time. In contrast, R2 showed the highest percentage of particles passing the y-midplane (100%) and 24% of particles passing through the breathing plane. The particle clearance was the second worst result with only 77% of particles clearing. Therefore, it is inferred that the particle residence time within the test chamber is much higher for the R2 case. The particle residence time is an important criterion to consider when dealing with inhalation and exposure limits to undesirable particles.

Ventilation R1 is similar to R2 but closer to the humanoid. The flow field between the two are similar but the closer arrangement of the outlet to the humanoid allows the particles to exit more easily. This causes the particle dispersion throughout the room for R1 to be less while the number of particles that are cleared is greater. Case R3 has a 45° angled outlet pointing at the lathe and is located at the same distance away from the humanoid as R2. It was found that R3 had the highest clearance rate of particles, 92% and low percentages of particles that flowed through the y-midplane (70%) and breathing plane (3%). The best ventilation design cannot be simply stated because of the many parameters that are involved. However, by using the three measurements provided in Fig. 10, it can be deduced that R3 and F1 provide safer ventilation designs to reduce the likelihood of particle inhalation.

4. Conclusion

Wood processing tasks such as circular sawing and turning that is associated with woodturning operators produce particularly high exposure levels. Five different ventilation designs were considered with the aim of reducing the particle suspension within the breathing zone. Measurements to evaluate the efficiency of each ventilation design included total particle clearance and the percentage of particles crossing through the breathing plane. The clearance of the particles from the working environment is an important parameter when considering the effectiveness of ventilation designs for safer occupational health. However, the percentage of particles that cross the breathing plane is of greater significance as this measurement provides a better determination of exposure levels. It was found that ventilation R3, where the local outlet emanated from the roof and had an angled outlet, provided greatest total particle clearance and low particles in the breathing plane. Additionally, F1 also provided low particles in the breathing plane but with less particle clearance suggesting that particles are being caught on surfaces. It was found that the airflow that was predominantly along the ceiling was affected significantly by the obstructing local roof ventilations (R1, R2, R3). The obstruction caused separation of the air which produced a complex flow region near the outlet. The study provides a benchmark for further investigation into the effects of particle size and density on the particle flow patterns and potential inhalation conditions for a given ventilation design. Additionally, the inclusion of heat transfer and thermal plumes generated from the human body, surrounding lighting and possible sunlight radiation will be included.

References

[1] Enarson DA, Chan-Yeung M. Characterization of health effects of wood dust exposures. American Journal of Industrial Medicine 1990;17:33–8.
[2] IARC/W.H.O. I.A.R.C monographs on the evaluation of carcinogenic risks to humans. Vol. 62: wood dust and formaldehyde. International Agency for Research on Cancer/World Health Organization; 1995.
[3] Dilworth M. Wood dust survey 1999/2000 final report. Health and Safety Laboratory, Crown; 2000.
[4] Demers P, Boffette P. Cancer risk from occupational exposure to wood dust: a pooled analysis of epidemiological studies. IARC Technical Report No. 30; 1998. p. 30.
[5] Chung KYK, Cuthber RJ, Revell GS, Wassel SG, Summer N. A study on dust emission, particle size distribution and formaldehyde concentration during machining of medium density fibreboard. Annals of Occupational Hygiene 2000;44:455–66.
[6] Wickham F. Air filters. Australia, AIRH, 1992 (No. DA 15).
[7] Tian ZF, Inthavong K, Tu JY. Deposition of inhaled wood dust in the nasal cavity. Inhalation Toxicology 2007;19(14):1155–65.
[8] Holmberg S, Li Y. Modelling of the indoor environment-particle dispersion and deposition. Indoor Air 1998;8:113–22.

[9] Lu W, Howarth AT. Numerical analysis of indoor aerosol particle deposition and distribution in two-zone ventilation system. Building and Environment 1996;31(1):41–50.

[10] Tian ZF, Tu JY, Yeoh GH, Yuen RKK. Numerical studies of indoor airflow and particle dispersion by large eddy simulation. Building and Environment 2007;42:3483–92.

[11] Srebric J, Vukovic V, He G, Yang X. CFD boundary conditions for contaminant dispersion, heat transfer and airflow simulations around human occupants in indoor environments. Building and Environment 2008;43:294–303.

[12] Madsen U, Breum NO, Nielsen PV. A numerical and experimental study of local exhaust capture efficiency. Annals of Occupational Hygiene 1993;37(6):593–605.

[13] Deevey M, Sinai Y, Everitt P, Voigt L, Gobeau N. Modelling the effect of an occupant on displacement ventilation with computational fluid dynamics. Energy and Buildings 2008;40:255–64.

[14] Murakami S, Kato S, Zeng J. Combined simulation of airflow, radiation and moisture transport for heat release from a human body. Building and Environment 2000;35:489–500.

[15] Murakami S. Analysis and design of the micro-climate around the human body with respiration by CFD. Indoor Air 2004;14:144–56.

[16] Morsi SA, Alexander AJ. An investigation of particle trajectories in two-phase flow systems. Journal of Fluid Mechanics 1972;55(2):193–208.

[17] Ounis H, Ahmadi G, McLaughlin JB. Brownian diffusion of submicrometer particles in the viscous sublayer. Journal of Colloid and Interface Science 1991;143(1):266–77.

[18] Crowe CT, Sommerfeld M, Tsuji Y. Multiphase flows with droplets and particles. Boca Raton, FL: CRC Press; 1998.

[19] Li A, Ahmadi G. Dispersion and deposition of spherical particles from point sources in a turbulent channel flow. Aerosol Science and Technology 1992;16:209–26.

[20] Macinnes JM, Bracco FV. Stochastic particle dispersion modeling and the tracer particle limit. Physics of Fluids A 1992;4:2809–23.

[21] ASHRAE. Ventilation and infiltration: ventilation and filtration. In: ASHRAE handbook 2001 fundamentals. Atlanta: American Society of Heating, Refrigeration and Air Conditioning Engineers Inc.; 2001.

[22] Dai YT, Juang YJ, WU YY, Breysse PN, Hsu DJ. In vivo measurements of inhalability of ultralarge aerosol particles in calm air by humans. Journal of Aerosol Science 2006(37):967–73.

[23] Chen Q. Comparison of different k–ε models for indoor airflow computations. Numerical Heat Transfer, Part B, Fundamentals 1995;28:353–69.

[24] Rhodin P, Moshfegh B. Numerical predictions of indoor climate in large industrial premises. A comparison between different k–ε models supported by field measurements. Building and Environment 2007;42:3872–82.